Available online at www.sciencedirect.com
SCIENCE DIRECT
Catalysis Today 105 (2005) 709–717
CATALYSIS TODAY
www.elsevier.com/locate/cattod

Comparison among structured and packed-bed reactors for the catalytic partial oxidation of CH_4 at short contact times

Matteo Maestri, Alessandra Beretta *, Gianpiero Groppi, Enrico Tronconi, Pio Forzatti

NEMAS—Centro di Eccellenza per l'Ingegneria dei Materiali e delle Superfici Nanostrutturate, Dipartimento di Chimica, Materiali e Ingegneria Chimica "Giulio Natta", Politecnico di Milano, Piazza Leonardo da Vinci 32, 20133 Milano, Italy

Abstract

Three types of catalyst support (foams, honeycomb monoliths with square channels and spheres with approximately equal values of specific geometric surface a_v) were examined and compared by simulation with a 1D, dynamic heterogeneous mathematical model for application to the autothermal partial oxidation of methane. Both cold start-up and steady-state behaviours were investigated.

It was found that mass and, particularly, heat transfer properties markedly affect the reactor behaviour, both at start up and at steady state. Thus, the choice of the catalyst support can lead to greatly different reactor performances. Concerning the reactor start-up, simulations revealed that better interphase heat transport properties and lower bed heat capacity are useful to minimize the total start-up time; on the other hand, more favourable transport properties reduce the maximum flow rate which allows to achieve and maintain an ignited steady state. At steady state, oxygen conversion is strictly governed by interphase mass transfer, while methane conversion depends on a more complex, mixed chemical-diffusional regime.

Keywords: Reactors; Catalytic partial oxidation; CH_4

1. Introduction

The catalytic partial oxidation of methane to CO and H_2 has been studied since the 1940s as an alternative to the commercial processes for synthesis gas production. Renewed interest in this technology was stimulated by Schmidt and coworkers [1,2] who first reported that excellent conversions and selectivities to syngas could be obtained in autothermal short contact time reactors, using Pt and Rh in various structured configurations. During the past 15 years several authors have confirmed that noble metal-based catalysts are highly active in converting methane to CO and H_2; very high yields can be obtained at few milliseconds contact times by operating at high reaction temperatures, which in turn can be accomplished by running the process adiabatically [3]. The possibility to produce H_2/CO mixtures without external energy input, in small reactors with reduced heat capacity makes the catalytic partial oxidation of methane and higher hydrocarbons a promising solution for novel small-scale applications of syngas. Stationary applications include the production of H_2-rich streams for the fuelling of hydrogen-driven vehicles or residential cogeneration systems, but also for the enhancement of gas turbines performances through the development of H_2-stabilized combustors. On board applications are also presently studied, such as the fuelling of SOFC-based Auxiliary Power Units or the shortening of the cold-start phase of catalytic mufflers through syngas oxidation.

Because of the severe operating conditions (characterized by high temperature and high flow rates), heat and mass transfer properties are expected to play a decisive role in the behaviour of short contact time partial oxidizers. In principle, the choice of catalyst support can greatly affect the reactor performances. Crucial aspects related to the various proposed applications are on one side the reactor

* Corresponding author.
E-mail address: alessandra.beretta@polimi.it (A. Beretta).

0920-5861/$ – see front matter © 2005 Elsevier B.V. All rights reserved.
doi:10.1016/j.cattod.2005.06.045

Nomenclature

a_v	specific area per unit volume (m^{-1})
A	reactor cross section (m^2)
$\hat{c}_p$	specific heat (J/kg/K)
d_{cell}	pore dimension (m)
d_{sphere}	sphere diameter (m)
d_{str}	foam strut equivalent cylinder diameter (m)
f	friction factor
G	superficial mass flow rate ($kg/m^2/s$)
h	heat transfer coefficient ($W/m^2/K$)
ΔH_j^R	heat of reaction (J/mol)
I_{cell}	cubic cell dimension (m)
k_{ax}	solid thermal conductivity (W/m/K)
k_{ax}^{eff}	effective solid thermal conductivity (W/m/K)
$K_{mat,i}$	mass transfer coefficient (m/s)
L_{rct}	reactor length (m)
p	pressure (Pa)
r_j	j-reaction rate ($mol/kg_{cat}/s$)
t	time (s)
T	temperature (K)
z	reactor axial coordinate (m)

Greek letters

ε	bed void fraction
ε_s	emissivity
ξ	volumetric catalytic fraction
ρ	density (kg/m^3)
σ	Stefan–Boltzmann constant
ω	weight fraction

Subscripts and superscripts

g	gas phase
s	solid phase
eff	effective

steady-state performance at high space velocity (in terms of conversion and selectivity), on the other side the reactor dynamic response especially during light-off.

While several catalyst configurations were proposed in the literature (including gauzes, foam monoliths, extruded honeycomb monoliths and spheres), the specific effects of the catalyst configuration and geometry were not systematically explored. Bodke et al. [4] have studied the performances of foam catalysts and reported that the addition of a washcoat layer prior to Rh deposition enhanced methane conversion and H_2 selectivity. The effect was associated to the increased surface area of Rh. They also investigated the effect of the foam cell density and found that smaller pore sizes gave better syngas yields. This was related to the progressive enhancement of mass transfer coefficients with decreasing pore size. Qualitatively, the data by Bodke et al. [4] seem to indicate that both the chemical reaction at the catalyst surface and the diffusion of reactants from the bulk gas-phase were kinetically important steps, so that the autothermal reactors operated under a mixed chemical-diffusion regime.

In a more recent work, Hohn and Schmidt [5] have compared the performances of Rh-coated foam monoliths and Rh-coated spheres at very high space velocity. It was found that on foams, syngas selectivity dropped as space velocity was increased above $4 \times 10^5\ h^{-1}$, while the use of dense spheres as supports allowed high conversions and selectivities even above $10^6\ h^{-1}$. These results were rationalized on the basis of the different heat transfer properties of the two support geometries. It was proposed that the enhanced convective heat transfer of foams favored the progressive cooling of the inlet portion of the bed at increasing space velocity, eventually leading to reactor blow-out.

The data by Hohn and Schmidt [5] over spheres and analogous data reported by Basini et al. [6,7] were theoretically analyzed by Bizzi et al. [8,9], but a quantitative comparison between spheres and foam was not addressed.

Concerning the dynamics of partial oxidation, important results are provided by the recent work of Deutschmann and coworkers [10], who developed a detailed model of a honeycomb monolith reactor and compared the numerical study with experimental observations.

In this work, the previous studies are extended and the comparative investigation of methane partial oxidation over different types of ceramic supports is addressed. Foams, honeycomb monoliths with square channels and spheres were analyzed by the means of a 1D dynamic heterogeneous model, wherein the intrinsic reaction kinetics were accounted for after the results of an independent kinetic study of the process and specific heat and mass transfer correlations were included for the different catalyst configurations. Aim of the work is the analysis of the combined effect of chemical reaction and heat and mass transfer properties on the dynamic and steady-state performances of an adiabatic reactor at high flow rates; the reactor response during start up and the effect of increasing the space velocity on reactants conversion and syngas selectivity were investigated for each configuration up to the limit of reactor blow-out.

2. Mathematical model

2.1. Assumptions and governing equations

A dynamic heterogeneous 1D model of a fixed bed adiabatic catalytic reactor was developed, which implements molecular, pseudo-steady-state kinetics. The model includes the species mass balances and the energy balances for the gas and solid phases, as well as the momentum balance: accumulation terms were considered in all equations but in the mass balances for the solid phase because of the smaller volume of the fluid in catalyst pores

Table 1
Model equations

Gas phase

Species mass balance equations:

$$\frac{\partial \omega_i}{\partial t} = -\frac{G}{\rho_g \cdot \varepsilon}\frac{\partial \omega_i}{\partial z} - \frac{a_v}{\varepsilon}K_{\mathrm{mat},i}(\omega_i - \omega_{i,\mathrm{wall}})$$

Energy balance equation:

$$\frac{\partial T_g}{\partial t} = -\frac{G}{\rho_g \varepsilon}\frac{\partial T_g}{\partial z} - \frac{a_v}{\rho_g \varepsilon \hat{c}_{p,g}}h(T_g - T_s)$$

$$\frac{\partial T_g}{\partial t} = -\frac{G}{\rho_g \cdot \varepsilon}\cdot\frac{\partial T_g}{\partial z} - \frac{a_v}{\varepsilon}\cdot h \cdot \frac{1}{\rho_g \cdot \hat{c}_{p,g}}\cdot(T_g - T_s)$$

Momentum balance equation:

$$\left(-\frac{1}{\rho_g} + \frac{G^2}{\rho_g^2 \cdot p}\right)\frac{\mathrm{d}p}{\mathrm{d}z} - \frac{G^2}{\rho_g^2 \cdot T_g}\frac{\mathrm{d}T_g}{\mathrm{d}z} = \frac{1}{2}\frac{G^2}{\rho_g^2}a_v f$$

Solid phase

Species mass balance equation:

$$0 = a_v \rho_g K_{i,\mathrm{mat}}(\omega_i - \omega_{i,\mathrm{wall}}) + \left(\sum_{j=1}^{NR}\nu_{i,j}r_j^{\mathrm{eff}}\right)\mathrm{MW}_i\rho_s\xi$$

Energy balance equation:

$$\frac{\partial T_s}{\partial t} = a_v h(T_g - T_s)/\left(\rho_s \hat{c}_{p,s}(1-\varepsilon)\right) + k_{\mathrm{ax}}^{\mathrm{eff}}/\left(\rho_s \hat{c}_{p,s}\right)\frac{\partial^2 T_s}{\partial z^2} + \left(\sum_{j=1}^{NR}(-\Delta H_j^R)r_j^{\mathrm{eff}}\right)\xi/\left(\hat{c}_{p,s}(1-\varepsilon)\right)$$

Boundary conditions

Reactor inlet ($z_1 = 0$)

$$\omega_{i,z=z1} = \omega_{i,\mathrm{feed}} \quad T_{g,z=z_1} = T_{\mathrm{feed}} \; p_{z=z_1} = p_{\mathrm{feed}}$$

$$-k_{\mathrm{ax}}^{\mathrm{eff}}\left.\frac{\partial T_s}{\partial z}\right|_{z_1} = \sigma\varepsilon_s(T_g^4 - T_s^4|_{z_1})$$

Reactor outlet ($z_2 = L_{\mathrm{rct}}$)

$$\left.\frac{\partial T_g}{\partial z}\right|_z = 0$$

$$-k_{\mathrm{ax}}^{\mathrm{eff}}\left.\frac{\partial T_s}{\partial z}\right|_{z_2} = -\sigma\varepsilon_s(T_g^4 - T_s^4|_{z_2})$$

Initial conditions

$$\omega_i(z,0) = 0;\; T_g(z,0) = T_{g,\mathrm{feed}};\; T_s(z,0) = T_{\mathrm{room}}$$

Table 2
Transport correlations

Foam (Giani et al. [14])

$$Nu = 0.9 \cdot Re^{0.42} \cdot Pr^{0.333}$$

$$Sh = 1.1 \cdot Re^{0.43} \cdot Sc^{0.333}$$

$$f = \left(0.87 + \frac{13.65}{Re}\cdot\left(\frac{l_{\mathrm{cell}} - d_{\mathrm{str}}}{l_{\mathrm{cell}}}\right)^2\right);\quad Re = \frac{d_{\mathrm{str}}\cdot G}{\mu}$$

Honeycomb monolith (Shah and London, [15])

$$Nu = 2.977 + \left(8.827 \cdot (10^3 \cdot Z^*)^{-0.545}\right)\cdot\exp(-48.2 \cdot Z^*)$$

$$Sh = 2.977 + \left(8.827 \cdot (10^3 \cdot Z^*)^{-0.545}\right)\cdot\exp(-48.2 \cdot Z^*)$$

$$Z^* = \frac{z}{d_{\mathrm{cell}}\cdot Re\cdot Pr} \text{ for } Nu;\quad Z^* = \frac{z}{d_{\mathrm{cell}}\cdot Re\cdot Sc} \text{ for } Sh$$

$$f = \frac{14.3}{Re};\quad Re = \frac{d_{\mathrm{cell}}\cdot G}{\mu\cdot\varepsilon}$$

Packed bed of spheres (Yoshida et al. [16] and Ergun [17])

$$j_h = j_d = 0.91 \cdot Re^{-0.51} \text{ for } Re < 50$$

$$j_h = j_d = 0.61 \cdot Re^{-0.41} \text{ for } Re > 50$$

$$f = \frac{(1-\varepsilon)^2}{\varepsilon^3}\cdot\frac{75}{d_{\mathrm{sphere}}\cdot G}\cdot\mu + \frac{7}{8}\cdot\left(\frac{1-\varepsilon}{\varepsilon^3}\right);\quad Re = \frac{d_{\mathrm{sphere}}\cdot G}{6\cdot(1-\varepsilon)\cdot\mu}$$

as compared to the bulk fluid volume. Preliminary simulations showed that the relevance of the dynamics of the gas phase is negligible, nevertheless the inclusion of the accumulation term in the equations improved the stability of the numerical solution. Model equations, boundary and initial conditions are listed in Table 1.

Due to the high axial Peclet number, axial diffusion was neglected in the gas phase. Homogeneous reactions were neglected, following the results reported in [10–13].

The bed transport properties were accounted for by specific heat and mass transfer correlations for each support [14–17], which are listed in Table 2. Notably, different characteristic dimensions are used depending on the type of support, namely particle diameter for packed beds; equivalent channel diameter for honeycombs; strut diameter for foams.

Concerning the solid phase, thermal conduction was accounted for by means of effective axial thermal conductivities, $k_{\mathrm{ax}}^{\mathrm{eff}}$. For the packed bed the correlations by Specchia et al. [18] and by Kunii and Smith [19] were applied for estimating the static and radiative contributions, respectively. For the monolith, a radiative contribution was accounted for by using the correlation from Lee and Aris [20]. For the foam, the correlation of Fourie and Du Plessis [21] was used; this was corrected by addition of a radiative contribution, that, in the absence of specific correlations, was estimated in analogy with the case of monoliths.

Simulations accounted for the presence of an inert portion (20% of the active length) of support prior to the catalytic bed; the use of radiation shields upstream and downstream from the catalytic bed is in fact common in the experimental practice, in order to realize the reactor axial insulation. A step profile of the catalytic washcoat along the reactor axial coordinate was accordingly assumed. Also, radiative axial dispersion at the reactor boundaries was considered.

In the solid-phase mass balance equations, effective reaction rates were considered. The a priori solution of the diffusion and reaction problem at a fixed reactor axial position (z) within the catalytic washcoat pointed out that the intraporous diffusional resistances for oxygen were greater by several orders of magnitude than for other species. Thus, intraporous diffusional resistances were accounted for by isothermal effectiveness factors only for combustion reactions, using the generalized Thiele modulus method [22].

Thermal properties ($\hat{c}_p$, ΔH_r°, ΔG_r°) were estimated according to the CHEMKIN correlations [23] and gas properties were calculated according to the correlations reported in [24].

2.2. Numerical method

The model consists of 15 PDEs equations and was solved numerically by the method of lines. The axial reactor length was split into a suitable number of grid points and in each point the spatial derivates were approximated by the Euler Backward differentiation method. Thus, from a 15 PDEs problem, a $15 \times n_{\mathrm{grid\ points}}$ DAE system was obtained.

The DAE system was solved by the initial value C++ Class BzzDae for stiff problems [25] of the BzzMath 5.0

Table 3
Kinetic scheme

Reaction	Rate expression (mol/kg$_{cat}$/s) − p_i (atm)	k_i (773 K)	$E_a/R \times 10^3$ (K)
$CH_4 + 2O_2 \rightarrow CO_2 + 2H_2O$	$r_1 = \frac{k_1 p_{CH_4}}{(1+K_{H_2O} p_{H_2O})^2}$	2.945	6.795
$CH_4 + H_2O \leftrightarrow CO + 3H_2$	$r_2 = \frac{k_2 p_{CH_4} (1-K_{p,2}/K_{eq,2})}{(1+K_{CO} p_{CO}+K_{O_2} p_{O_2})^2}$	2.175	7.069
$CH_4 + CO_2 \leftrightarrow 2CO + 2H_2$	$r_3 = \frac{k_3 p_{CH_4} (1-K_{p,3}/K_{eq,3})}{(1+K_{CO} p_{CO}+K_{O_2} p_{O_2})^2}$	2.175	7.069
$CO_2 + H_2 \leftrightarrow CO + H_2O$	$r_4 = \frac{k_4 p_{CO_2} p_{H_2} (1-K_{p,4}/K_{eq,4})}{(1+K_{CO} p_{CO}+K_{O_2} p_{O_2})^2}$	3.4×10^2	3.91
$H_2 + 0.5O_2 \rightarrow H_2O$	$r_5 = k_5 p_{H_2}$	2×10^3	5
$CO + 0.5O_2 \rightarrow CO_2$	$r_6 = k_6 p_{CO}$	90	7
O_2 adsorption		12×10^2	−7
H_2O adsorption		4.23	−19.9
CO adsorption		23.82	−3.12

library [26]. This integrator can exploit the tridiagonal block structure of the Jacobian and resulted very efficient and robust.

Convergence of the solution was checked by varying the number of grid points along z (typically 250 was adequate) and by using the internal criteria of the DAE integrator.

2.3. Kinetic scheme

A steady-state molecular indirect-consecutive kinetic scheme of CH_4 partial oxidation over Rh catalysts was incorporated in the reactor model. The kinetic scheme was developed on the basis of a wide experimental campaign in annular reactor at high space velocity [27–29]. Herein, CH_4 partial oxidation tests, as well as CH_4 steam reforming and CO and H_2 fuel rich combustion tests were realized at varying temperature, flow rate, and feed composition far from thermodynamic equilibrium, under quasi-isothermal conditions and reduced impact of mass transfer limitations. All kinetic tests were run under diluted conditions; however reaction orders were substantially confirmed by tests at higher reactant concentration [29].

The heterogeneous reactions and the corresponding kinetic expressions are listed in Table 3. It should be noted that, in line with the experimental evidence, the developed expressions reproduce the kinetic independence of methane reaction rates from the surface concentration of co-reactants like O_2 or H_2O or CO_2. Such an assumption was extended to CO and H_2 combustions, which were assumed for simplicity as first order dependent on the fuel concentration only. In order to account for the limiting concentration of O_2 (and H_2O and CO_2), reaction rates were incorporated within the mass balances and multiplied by a "limiting" factor ϑ defined as:

$$\vartheta = \frac{p_i}{10^{-5} + p_i}$$

where p_i is the partial pressure of O_2 for combustion reactions and CO_2 or H_2O for reforming reactions.

Table 4
Supports properties

α-Al_2O_3	ρ (kg/m^3)	2000
	c_p (kJ/kg/K)	0.865
	k_s (W/m/K)	3
Foam	Type (ppi)	25
	ε	0.8
	a_v (1/m)	2760
Honeycomb monolith	Type (cpsi)	400
	ε	0.7
	a_v (1/m)	2800
Packed bed of spheres	d_{sphere} (m)	0.0013
	ε	0.4
	a_v (1/m)	2770

3. Results and discussion

Three different types of ceramic catalyst supports were analyzed in the present work (foam monolith, honeycomb monolith and spheres), all successfully applied in the literature for the autothermal partial oxidation of CH_4. Concerning the support geometries (summarized in Table 4 along with solid properties), configurations with approximately equal values of specific geometric surface ($a_v \cong 2800\ m^{-1}$) were selected: a 25 ppi foam with 0.8 void fraction; a honeycomb monolith with 1 mm channel opening and 0.7 void fraction; spheres with 1.3 mm diameter and 0.4 bed void fraction. The supports were considered as wash-coated and the same catalyst volume fraction (8.4%) was assumed for the three cases. Equal total reactor volume was assumed in the simulations, considering a disk shaped geometry with 0.03 m length and 0.085 m external diameter.

Fig. 1 compares the asymptotic values of the heat and mass transfer coefficients of the three configurations at increasing gas flow rate. The foam is characterized by the highest values of heat and mass transfer coefficients in the whole range of flow rates investigated. Concerning the other two support configurations, at low flow rate the monolith presents better transport properties than the packed bed, but,

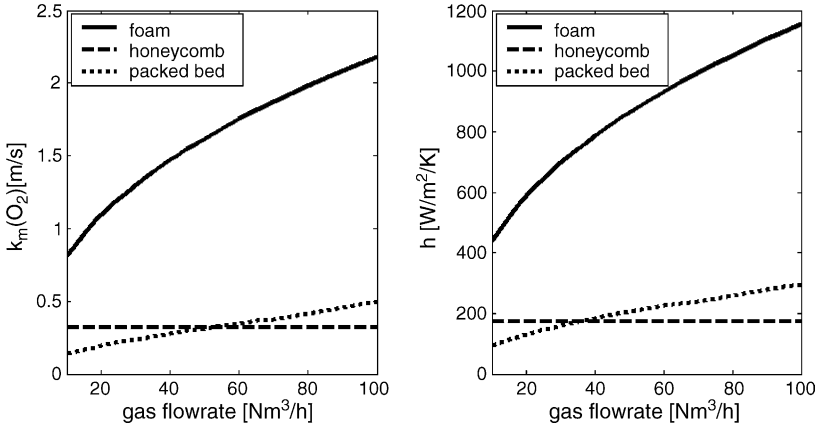

Fig. 1. Comparison of transport properties of different supports (T = 620 K; P = 1.5 bar).

at increasing gas flow rate, the transport coefficients of the packed bed overcome those of the monolith due to the negligible dependence of the latter on gas velocity.

3.1. Reactor start-up

Cold start conditions, with the initial solid temperature fixed at 298 K, were investigated; an inlet feed temperature of 620 K, a methane/air feed mixture with O_2/CH_4 = 0.6 (v/v) and a total pressure of 1.5 bar were assumed. This case reproduces a light-off strategy wherein the feed stream is initially preheated by an external source; it also represents a common experimental practice in the literature. It is noted that, concerning the gas inlet temperature, 620 K was preliminarily identified as the minimum value that secured ignition of all the three supports at the gas flow rate of 10 N m^3 h^{-1}.

It was found that for each catalyst configuration the reactor start-up is characterized by the initial progressive heating of the solid phase until ignition of methane combustion occurs on the catalytic surface, followed by the propagation of the reaction zone throughout the reactor. Fig. 2 reports the calculated evolution of the catalyst temperature in the case of the packed bed of spheres; the same qualitative behaviour was found also for the other two configurations. It is worth observing that, under the assumed operating conditions, the reactor ignition always started at the end of the bed and propagated upwards, in line with previous results about honeycomb monoliths [10]. However, as reported by Ramanathan et al. [30], it was found that the location of the ignition point strongly depends on the catalyst activity, that is, for a given catalyst, on the values of pressure, temperature, feed composition, and catalyst wash-coat thickness. For instance, assuming an inlet feed temperature of 650 K, the ignition started at the reactor inlet and propagated downstream. This is in line with the fact that before ignition, the reactor works in a chemically controlled regime. In particular, the dynamics of the solid temperature are driven by both the methane combustion reaction (heat release) and the gas–solid convective heat transfer (heat removal).

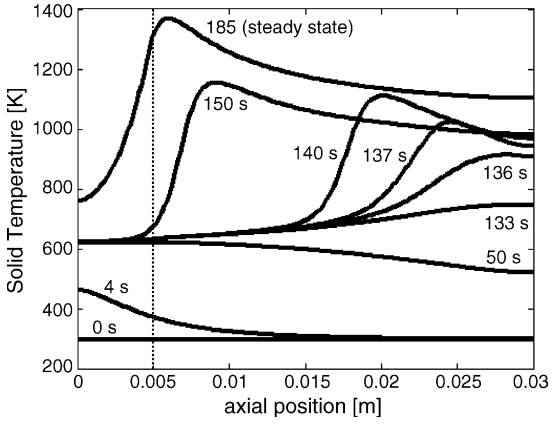

Fig. 2. Solid temperature evolution during start-up: packed bed support.

If the heat released by methane combustion is higher than the heat removed by the gas–solid heat transfer, then an increase of the solid temperature occurs: here, once the solid temperature reaches a sufficiently high value, a hot-spot establishes. In the case of 620 K feed temperature and back-end ignition, the same condition (solid heating and hot-spot growth) realizes successively upstream at each axial position; as a result, the hot-spot "moves" from the ignition point and propagates towards the inlet bed section.

The progressive heating of the catalytic bed is accompanied by the rapid consumption of O_2 and the progressive consumption of CH_4 with formation of synthesis gas. As a consequence of the indirect consecutive kinetic scheme adopted in this work, axial profiles of reaction rates at steady state (herein not reported) show that most of the O_2 consumption occurs in correspondence of the inlet hot-spot, while methane conversion and syngas production proceed mostly beyond the hot-spot over the entire length of the reactor. The final temperature profile is determined by the combination of several physical phenomena in addition to the chemical reactions; these include the quenching effect of the feed cold gas, the rate of mass transfer which controls O_2 consumption, the axial thermal dispersion which smoothens

the temperature peak, the interphase heat transfer which influences the solid temperature downstream from the hot-spot.

As reported in a previous work [31], if inlet conditions are such that the heat removed is enough to quench the heat released by the initial surface reaction, the reactor start-up does not occur. As a result, for each catalyst configuration and a given feed inlet temperature an upper limit of the gas flow rate exists at start-up, above which ignition is prevented. Such an upper limit increases on going from foam, to honeycomb, to spheres following the corresponding decreasing trend of the heat transfer rate, i.e. of the quenching ability of the gas stream. At the conditions assumed, it was found that the maximum gas flow rates at start up for the three supports are the following: 10 N m^3 h^{-1} for foam, 18 N m^3 h^{-1} for honeycomb and 20 N m^3 h^{-1} for packed bed.

The total start-up characteristic time is the sum of the ignition and propagation times: the first consists of the heat-up time required for the solid to reach the methane combustion ignition temperature; the second consists of the time required by the hot ignited zone to propagate throughout the reactor. At 10 N m^3 h^{-1} and 620 K inlet temperature, the total start-up times were: 50 s for foam, 85 s for monolith and 185 s for packed bed. Ignition, which is closely related to the heat capacity and the gas–solid heat transfer of the bed, was found as the slower phenomenon; in the packed bed reactor (characterized at start-up by the lowest gas–solid heat transfer and the highest heat capacity) it occurred after 136 s, and was progressively faster in the monolith (58 s) and in the foam (29 s).

3.2. Steady-state: effect of gas flow rate

After ignition and reach of steady state, the cooling of the gas inlet temperature down to 300 K was simulated; in this condition, the effect of a progressive increase of the flow rate was investigated. At each value of flow rate, steady-state conditions were verified by simulating a time interval of 1000 s. The effect was analyzed in the range of 10 N m^3 h^{-1} to 100 N m^3 h^{-1} (corresponding to a range of 5.9×10^4 to 5.9×10^5 h^{-1} in terms of space velocity referred to the total reactor volume) or up to the limit of reactor extinction. In the case of the foam, in fact, blow-out occurred at approximately 2.46×10^5 h^{-1}; at this space velocity, a slow shift of the hot-spot towards the bed exit was observed, which eventually led to the extinction of the reaction. Steady-state conversions dropped to zero. In the cases of honeycomb and packed bed, simulations on the effect of flow rate could be extended up to 100 N m^3 h^{-1} without occurrence of blow-out. This effect can be explained by considering, as already shown in Fig. 1, that the increase of gas flow rate results in the enhancement of the transport properties (both mass and heat). In the case of the foam the effect is such that at 2.46×10^5 h^{-1} the quench ability of the gas stream prevails over the heat released by the oxidation reactions.

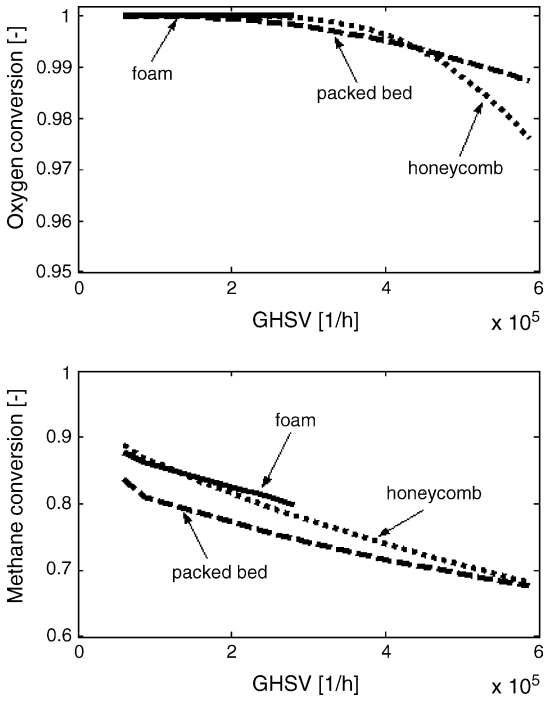

Fig. 3. Effect of GHSV on methane and oxygen conversions for the different supports.

As a general trend, at increasing space velocity a moderate decrease of O_2 conversion and a more important decrease of CH_4 conversion are observed, in line with the indirect nature of the kinetic scheme. Calculated trends are reported in Fig. 3. As a result of the selectivity loss, the increase of space velocity is accompanied by a significant increase of the process exothermicity; this is clearly shown in Fig. 4 where the axial temperature profiles of the solid phase for each configuration are plotted at two values of space velocity. Decrease of the contact time, enhancement of the heat and mass transfer coefficients and increase of the average solid temperature are thus the main factors associated with the increase of space velocity; their effects differently combine in the three configurations, thus determining differences in the final performances of foam, honeycomb and spheres. In Fig. 5, the gas temperature axial profile for each configurations is reported for a GHSV equal to 2.46×10^5 h^{-1}. In line with the exo–endothermic reaction sequence of the adopted kinetic scheme, the gas temperature is much lower than the solid one in the inlet hot spot region, where oxidation reactions occur, while downstream, where endothermic reactions prevail, the gas phase becomes slightly hotter than the solid one. As a whole, the gas temperature profile is considerably smoother than the solid one, without a pronounced hot spot.

In all the investigated conditions, according to our indirect consecutive kinetic scheme the rate of oxidation reactions is so fast that O_2 conversion is fully controlled by mass transfer in each reactor configuration. As a result, O_2 conversion is always complete in the foam reactor, while in the other configurations it slightly decreases with increasing

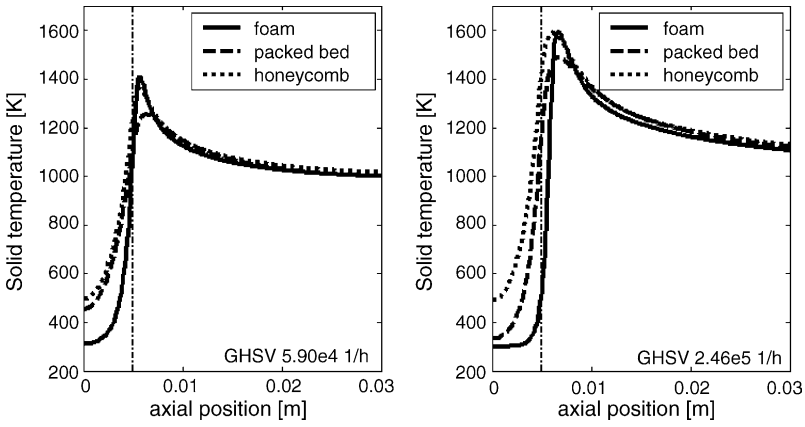

Fig. 4. Solid temperature profile of the different supports at two different GHSV.

space velocity and the relative trend is strictly related to the extent of mass transfer coefficient. In fact, O_2 conversion is higher in the honeycomb than in the packed bed up to intermediate values of space velocity, while it is higher in the packed bed at the highest values of GHSV investigated.

Concerning CH_4 conversions, on the other hand, the calculated trends result from a complex combination of the cited effects. Differently from O_2, CH_4 consumption is governed by a mixed chemical-diffusional regime: at the lowest space velocities (and lowest average catalyst temperatures) it is mainly chemically controlled, while at the highest values of GHSV (and temperature) investigated the role of mass transfer becomes more important. This can be appreciated by analyzing the axial concentration gradients of methane at varying space velocities. Fig. 6 shows such gradients in the case of the honeycomb catalyst, but the results are representative of all the configurations. Bulk and surface concentrations of methane are relatively close at $5.9 \times 10^4\ h^{-1}$, while the surface concentration has a dramatic drop at $5.9 \times 10^5\ h^{-1}$. Consequently, at the lowest space velocities the relative values of CH_4 conversion reflect the relative scale of the average solid temperature: conversion in the honeycomb results slightly higher than that in the foam, and both are much higher than CH_4 conversion in the packed bed; in fact the average temperature of the packed bed is penalized by the effect of thermal conductivity, which strongly reduces the hot-spot temperature. On increasing space velocity, the effect of mass transfer on methane conversion becomes progressively more important. As a result, the foam shows the highest values of conversions, while the performances of honeycomb and packed bed tend to become closer since the enhancement of mass transfer in the packed bed progressively compensates the difference in the hot-spot temperature with the honeycomb.

In line with experimental evidence [5], in conditions with oxygen conversion always close to 100%, it was also found that, at increasing space velocity, H_2 selectivity drops, while CO selectivity keeps approximately constant, as shown in Fig. 7. In the present simulations, this result can be related to the nature of the kinetic scheme; since at high flow rates O_2 conversion is not complete, then the relative amount of H_2 and CO is controlled by the relative rate of the consecutive combustions (with H_2 oxidation being much faster than CO oxidation) and not by chemical equilibria. However, it is worth emphasizing that such conclusions strongly depend on

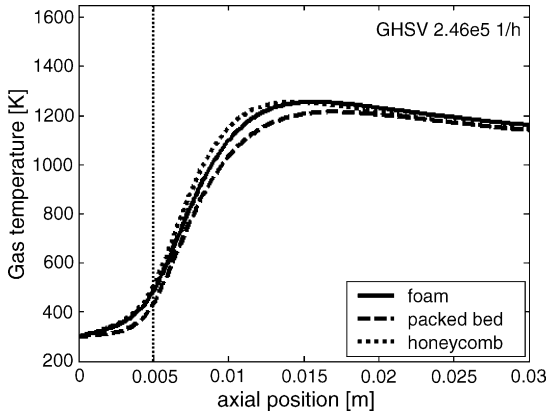

Fig. 5. Gas temperature profile of the different supports (GHSV = $2.46 \times 10^5\ h^{-1}$).

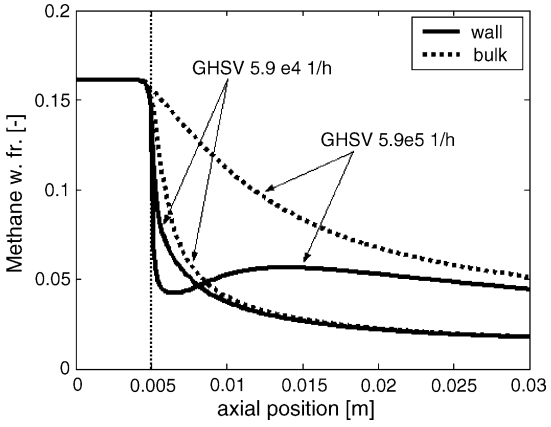

Fig. 6. Axial profile of CH_4 weight fraction at different GHSV for honeycomb monolith.

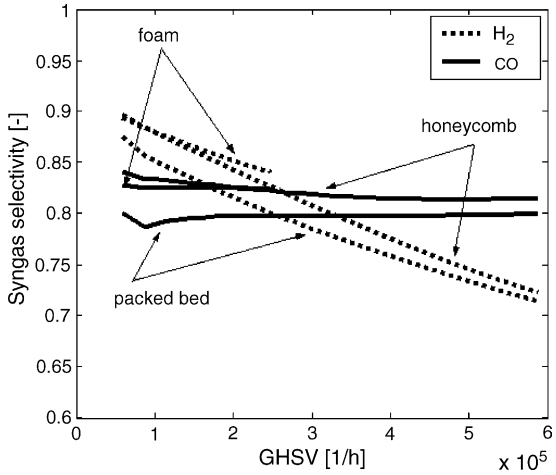

Fig. 7. Effect of GHSV on syngas selectivity for the different supports.

the assumed operating conditions; in a previous work [31], wherein a preheated inlet feed and 4 bar operating pressure were assumed, it was found that the product distribution was only slightly affected by flow rate and largely controlled by chemical equilibrium.

Simulations revealed that the pressure drop is an important issue only for packed bed, while for the other two support configurations it was found negligible over the entire range of assumed flow rates. The pressure drop for packed bed at the maximum flow rate was 0.36 bar, despite the high diameter to length ratio of the bed. Noteworthy shallow packed bed reactors – which have been suggested in the literature for methane partial oxidation [5] – may result in serious gas channelling.

4. Conclusion

Transport phenomena play a decisive role in the process of methane partial oxidation. Mass and, particularly, heat transfer properties markedly affect the reactor behaviour, both at start-up and at steady-state. Thus, the choice of catalyst support can lead to greatly different reactor performances.

Concerning the reactor start-up, simulations revealed that better interphase heat transport properties and lower heat capacity are useful to minimize the total start-up time (ignition and propagation); on the other hand, more favourable transport properties reduce the maximum flow rate which allows to achieve (ignition) and maintain (extinction) an ignited steady-state. Accordingly, the foam (characterized by the best transport properties) exhibited the shortest start-up time and the lowest value of the maximum gas flow rate.

At steady state, it was found that oxygen conversion is strictly governed by interphase mass transfer, while methane conversion depends on a more complex, mixed chemical-mass transfer regime: the chemically controlled regime prevails at lower flow rates, while at higher flow rates the role of mass transfer becomes of greater importance due to higher solid temperatures. In the present simulations, at the intermediate value of GHSV of $2.4 \times 10^5\ h^{-1}$, the foam performed slightly better than the honeycomb, both being significantly better than the packed bed. At the highest values of flow rates investigated, the enhancement of transport properties in the packed bed makes this support more competitive; however, pressure drop may become an issue.

On a more general basis, the present work points out the great sensitivity of the reactor behaviour upon the support characteristics; this offers a large number of degrees of freedom for reactor design and optimization, by proper tailoring of the type, the geometry and the material of the catalyst support.

Acknowledgements

This work was supported by MIUR-Italy and UE-contract ENK5-CT-2002-00683.

References

[1] D.A. Hickman, L.D. Schmidt, J. Catal. 138 (1992) 267.
[2] D.A. Hickman, E.A. Haupfear, L.D. Schmidt, Catal. Lett. 17 (1993) 223.
[3] P. Aghalayam, Y.K. Park, D.G. Vlachos, Catalysis 15 (2000) 98.
[4] A.S. Bodke, S.S. Bharadwaj, L.D. Schmidt, J. Catal. 179 (1998) 138.
[5] K.L. Hohn, L.D. Schmidt, Appl. Catal. A: Gen. 211 (2001) 53.
[6] L. Basini, A. Guarinoni, A. Aragno, Catal. Today 190 (2000) 284.
[7] L. Basini, K.K. Aasberg-Petersen, A. Guarinoni, M. Østberg, Catal. Today 64 (2001) 9.
[8] M. Bizzi, L. Basini, G. Saracco, V. Specchia, Ind. Eng. Chem. Res. 42 (2003) 62.
[9] M. Bizzi, G. Saracco, R. Schwiedernoch, O. Deutschmann, AIChE J. 50 (2004) 1289.
[10] R. Schwiedernoch, S. Tischer, C. Correa, O. Deutschmann, Chem. Eng. Sci. 58 (2003) 613.
[11] M. Bizzi, L. Basini, G. Saracco, V. Specchia, Chem. Eng. J. 90 (2002) 97.
[12] O. Deutschmann, L.D. Schmidt, AIChE J. 44 (1998) 2465.
[13] C. Appel, J. Mantzaras, R. Schaeren, R. Bombach, A. Inauen, N. Tylli, M. Wolf, T. Griffin, D. Winkler, R. Carroni, Proc. Combust. Inst. 30 (2005) 2509.
[14] L. Giani, G. Groppi, E. Tronconi, Ind. Eng. Chem. Res. 44 (2005) 4993.
[15] R.K. Shah, A.L. London, Laminar Flow Forced Convection in Ducts, Academic Press, New York, 1978.
[16] F. Yoshida, D. Ramaswami, O.A. Hougen, AIChE J. 8 (1962) 5.
[17] S. Ergun, Chem. Eng. Prog. 48 (1952) 89.
[18] V. Specchia, G. Baldi, S. Sicardi, Chem. Eng. Commun. 4 (1980) 361.
[19] D. Kunii, J.M. Smith, AIChE J. 6 (1960) 71.
[20] S.T. Lee, R. Aris, Chem. Eng. Sci. 32 (1977) 827.
[21] J.G. Fourie, J.P. Du Plessis, AIChE J. 50 (2004) 547.
[22] G.B. Froment, K.B. Bischoff, Chemical Reactor Analysis and Design, John Wiley and Sons, New York, 1990.
[23] R.J. Kee, F.M. Rupley, J.A. Miller, The CHEMKIN Thermodynamic Data Base, Report No. SAND87-8215B, Sandia National Laboratories, 1987.

[24] R.C. Reid, J.M. Prausnitz, B.E. Poling, The Properties of Gases and Liquids, fourth ed., McGraw Hill, New York, 1988.
[25] D. Manca, G. Buzzi-Ferraris, T. Faravelli, E. Ranzi, Combust. Theory Model. 5 (2001) 185.
[26] G. Buzzi-Ferraris, BzzMath 5.0, http://www.chem.polimi.it/homes/gbuzzi.
[27] I. Tavazzi, A. Beretta, G. Groppi, P. Forzatti, in: X. Bao, Y. Xu (Eds.), Proceedings of the Seventh Natural Gas Conversion Symposium on Studies in Surface Science and Catalysis, vol. 147, Elsevier, 2004, p. 163.
[28] I. Tavazzi, Ph.D. thesis, Politecnico di Milano, 2005.
[29] T. Bruno, A. Beretta, G. Groppi, M. Roderi, P. Forzatti, Catal. Today 99 (2005) 89.
[30] K. Ramanathan, D.H. West, V. Balakotaiah, Catal. Today 98 (2004) 357.
[31] M. Maestri, A. Beretta, G. Groppi, E. Tronconi, P. Forzatti, Chem. Eng. Trans. 6 (2005) 13.